

Nanoscale

Accepted Manuscript



This is an *Accepted Manuscript*, which has been through the Royal Society of Chemistry peer review process and has been accepted for publication.

Accepted Manuscripts are published online shortly after acceptance, before technical editing, formatting and proof reading. Using this free service, authors can make their results available to the community, in citable form, before we publish the edited article. We will replace this *Accepted Manuscript* with the edited and formatted *Advance Article* as soon as it is available.

You can find more information about *Accepted Manuscripts* in the [Information for Authors](#).

Please note that technical editing may introduce minor changes to the text and/or graphics, which may alter content. The journal's standard [Terms & Conditions](#) and the [Ethical guidelines](#) still apply. In no event shall the Royal Society of Chemistry be held responsible for any errors or omissions in this *Accepted Manuscript* or any consequences arising from the use of any information it contains.

ARTICLE

Seeing the Diabetes: Visual Detection of Glucose Based on the Intrinsic Peroxidase-Like Activity of MoS₂ nanosheets

Cite this: DOI: 10.1039/x0xx00000x

Tianran Lin, Liangshuang Zhong, Liangqia Guo*, Fengfu Fu and Guonan Chen^[a]Received 00th June 2014,
Accepted 00th June 2014

DOI: 10.1039/x0xx00000x

www.rsc.org/nanoscale

Molybdenum disulfide (MoS₂) has attracted increasing research interest recently due to the unique physical, optical and electrical properties correlated with its 2D ultrathin atomic layer structure. Until now, however, great efforts have focused on the applications in lithium ion batteries, transistors, hydrogen evolution reaction, et al. Herein, for the first time, MoS₂ nanosheets are discovered to possess an intrinsic peroxidase-like activity, and can catalytically oxidize 3,3',5,5'-tetramethylbenzidine (TMB) by H₂O₂ to produce a color reaction. The catalytic activity follows the typical Michaelis-Menten kinetics and is dependent on temperature, pH, H₂O₂ concentration, and reaction time. Based on this finding, a highly sensitive and selective colorimetric method for H₂O₂ and glucose detection is developed and applied to detect glucose in serum samples. Moreover, a simple, cheap, and portable test kit for the visual detection of glucose in normal and diabetes serum samples with instrument-free and simple operation is constructed by utilizing agarose hydrogel as a visual detection platform.

1. Introduction

Molybdenum disulfide (MoS₂), one of the transition metal dichalcogenides with two-dimensional (2D) layered structure analogous to graphene, has attracted increasing research interest recently.¹⁻⁶ MoS₂ is composed of three stacked atom layers (S-Mo-S) held together by van der Waals forces.^{2, 3, 7} Due to the weak van der Waals interaction between MoS₂ layers, which allows Li⁺ ions to diffuse without a significant increase in volume expansion, a number of different morphologies of MoS₂ were studied as a cathode material used in lithium ion batteries.^{8, 9} Unlike graphene, bulk MoS₂ is semiconducting with an indirect bandgap of 1.2 eV, whereas single-layer MoS₂ is a direct gap semiconductor with a bandgap of 1.8 eV.¹⁰ This transition from indirect band gap to direct band gap resulted in giant enhancement in photoluminescence quantum yield.^{10, 11} Single-layer MoS₂ at room temperature exhibits a high channel mobility (~200 cm² V⁻¹s⁻¹) and current ON/OFF ratio (1 × 10⁸) when it was used as the channel material in a field-effect transistor.⁷ Large carrier mobility as well as robust mechanical property makes MoS₂ an attractive material to fabricate the

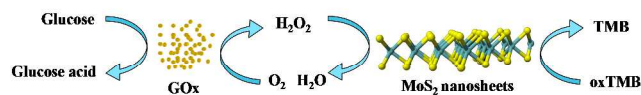
flexible single-layer or multilayer transistors, phototransistors, or field-effect transistors.¹²⁻²⁰ Extensive studies on the electro- and photoelectrocatalytic activity proved that MoS₂ could be a promising candidate as the catalyst of hydrodesulfurization,²¹ hydrogen evolution reaction,²²⁻²⁴ and biosensors.²⁵

Recently, colorimetric methods are particularly attractive for point-of-use applications because they can be visually and simply read out by the naked eyes.^{26, 27} For example, Au nanoparticles-based colorimetric assays have been widely used for detecting DNA,^{28, 29} protein,^{30, 31} small molecules,^{32, 33} metal ions,^{27, 34-36} anions.³⁷ Since no requirement for any sophisticated instrumentation is needed, colorimetric methods show great potential for portable and inexpensive daily life applications. To this end, enzyme-mimetic inorganic nanomaterials³⁸⁻⁴¹ have emerged as a new class of ideal and important tools for colorimetric detection owing to their high stability, easy preparation, controllable structure and composition, and tunable catalytic activity.³⁸ Enzyme mimetics possess many advantages over nature enzymes such as low cost, more stable against denature or protease digestion and have been applied in colorimetric bioassays and medical diagnostics.^{42, 43}

In this contribution, to the best of our knowledge, for the first time, we discovered that MoS₂ nanosheets possessed an intrinsic peroxidase-like catalytic activity. MoS₂ nanosheets could catalyze the reaction of peroxidase substrate 3,3',5,5'-tetramethylbenzidine (TMB) in the presence of H₂O₂ to produce a blue color reaction. Based on this finding, a highly sensitive and selective colorimetric method for H₂O₂ and

[a] Ministry of Education Key Laboratory of Analysis and Detection for food safety, Fujian Provincial Key Laboratory of Analysis and Detection Technology for Food Safety Department of Chemistry, Fuzhou University, Fuzhou, 350116, China, E-mail: lqguo@fzu.edu.cn, Fax: (+)86 591-22866135

glucose was developed (Scheme 1) and applied to detect glucose in human serum samples. Moreover, a simple, cheap, and portable test kit for the visual detection of glucose in normal and diabetes serum samples with instrument-free and simple operation was constructed as a proof of concept by utilizing agarose hydrogel as a visual detection platform.



Scheme 1. Schematic illustration of colorimetric detection of glucose by using glucose oxidase (GOx) and MoS₂ nanosheets-catalyzed reactions.

2. Results and Discussion

2.1 Characterization of MoS₂ nanosheets

Fig.S1(A) showed TEM image of layered MoS₂ nanosheets. The HRTEM image (Fig.S1(B)) showed the periodic atom arrangement of the MoS₂ nanosheets with a layer separation about 0.62 nm. TEM-based EDX analysis (Fig.S1(C)) revealed there was no other metal impurity in the sample. Two typical peaks at 627 nm and 672 nm, which can be attributed to the characteristic A1 and B1 direct excitonic transitions of MoS₂ with the energy split from the valence band spin-orbital coupling,⁵ were observed in the UV-visible absorption spectrum of diluted MoS₂ nanosheets dispersion (Fig.S1(D)). The XPS Mo 3d core-level spectrum (Fig.S1(E)) showed two peaks at 229.1 and 232.1 eV, attributed to the doublet Mo 3d_{3/2} and Mo 3d_{5/2}, respectively.^{4,11} The peaks at 163.2 and 161.9 eV in the XPS S 2p core-level spectrum (Fig.S1(F)) were corresponding to the S 2p_{1/2} and S 2p_{3/2} orbits of divalent sulfide ions (S²⁻).^{4,11} A typical AFM image and height profiles of MoS₂ nanosheets with sizes ranging from tens to hundreds of nanometers and thickness of 3 ~ 4 nanometers due to the overlap of multilayer MoS₂ nanosheets^{6, 14} were showed in Fig.S1(G, H, I). SEM-based EDX analysis (Fig.S1(J)) confirmed the component and stoichiometry of MoS₂ nanosheets with a Mo/S atomic ratio of ~ 1:2.

2.2 Peroxidase-like activity of MoS₂ nanosheets

The peroxidase-like activity of MoS₂ nanosheets was firstly evaluated by the catalytic oxidation of peroxidase substrate TMB in the presence of H₂O₂. As shown in Fig.1A, only addition of H₂O₂ or MoS₂ nanosheets to TMB solution the absorbance at 652 nm displayed negligible change, indicating no oxidation reaction occurred. However, upon addition of MoS₂ nanosheets and H₂O₂ to TMB solution, the color of the

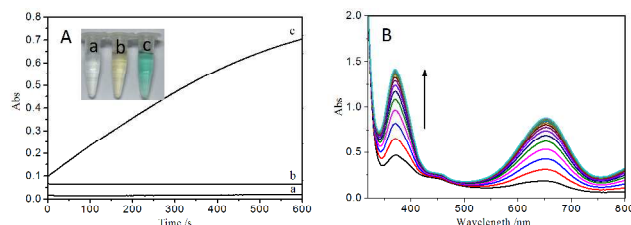


Fig.1 (A) Time-dependent absorbance changes at 652 nm of TMB solution in different reaction systems. (a) TMB + H₂O₂, (b) MoS₂ nanosheets + TMB, and (c) MoS₂ nanosheets + TMB + H₂O₂. Inset are the photos of reaction system (a), (b), and (c), respectively. (B) The UV-visible absorption spectra change in the system of MoS₂ nanosheets + TMB + H₂O₂ with the reaction time. Concentration of MoS₂ nanosheets, TMB, and H₂O₂ were 1.8 μg mL⁻¹, 1.2 mmol L⁻¹, 0.04 mmol L⁻¹, respectively.

mixture solution was turning from pale yellow to yellow-green, blue-green, blue (Fig.S2) and the absorbance at 652 nm was increasing with the reaction time, which indicated MoS₂ nanosheets could catalyze the oxidation of TMB by H₂O₂ to produce a typical deep-blue color, and the solution exhibited intense characteristic absorbance at 369 and 652 nm (Fig.1B), which are ascribed to the charge-transfer complexes derived from the one-electron oxidation of TMB (oxTMB).³⁸⁻⁴¹ This color reaction is also quenched by adding H₂SO₄.⁴⁴ After catalytic reaction the morphology of MoS₂ nanosheets almost unchanged according to TEM image (Fig.S3(A)), HRTEM image (Fig.S3(B)), AFM image (Fig.S3(F)) and AFM height profiles (Fig.S3(G, H)), SEM image and S and Mo mapping (Inset of Fig.S3(I)). The XPS analyses (Fig.S3(D, E)) showed the valence state of Mo and S remained +4 and -2, respectively. TEM-based and SEM-based EDX analyses (Fig.S3(C) and S3(I)) demonstrated the component and stoichiometry of MoS₂ nanosheets remained unchanged. These results indicated MoS₂ nanosheets exhibited an intrinsic peroxidase-like activity and both MoS₂ nanosheets and H₂O₂ were required for the reaction, as is the case for horseradish peroxidase (HRP). The peroxidase-like activity of MoS₂ nanosheets was further confirmed by the catalytic oxidation of other peroxidase substrates such as 2,2'-azino-bis(3-ethylbenzothiazoline-6-sulfonic acid) diammonium salt (ABTS) and *O*-phenylenediamine (OPD) in the presence of H₂O₂. Fig.S4 showed that MoS₂ nanosheets could catalyze ABTS to give a green color and catalyze OPD to give an orange color.

The peroxidase-like activity of MoS₂ nanosheets was further investigated by selecting the substrates TMB and H₂O₂ as a model reaction system. Fig.S5 showed the time-dependent absorbance changes against concentrations of MoS₂ nanosheets. The increasing concentration of MoS₂ nanosheets could improve the reaction rate. Similar to IIRP, the catalytic activity of MoS₂ nanosheets was found to be dependent on temperature, pH, H₂O₂ concentration, and reaction time (Fig.S6). MoS₂ nanosheets showed a high catalytic activity over a wide pH (2.0-7.5), which is wider than that of other peroxidase mimetics, such as MIL-53(Fe),³⁸ Co₃O₄,⁴⁰ TiO₂ nanotubes,⁴¹ Fe₃O₄ NPs,⁴⁴ Pt nanotubes,⁴⁵ Fe-Co alloy NPs,⁴⁶ ZnFe₂O₄ NPs,⁴⁷ graphene oxide,⁴⁸ carbon nanodots,⁴⁹ carbon nitride dots,⁵⁰ SWCNT.⁵¹ The wide pH range should be beneficial for the application of MoS₂ nanosheets. The optimal pH, temperature, H₂O₂ concentration, reaction time were approximately 6.9, 30 °C, 150 mmol L⁻¹, and 30 min, respectively.

The peroxidase-like catalytic property of MoS₂ nanosheets was further investigated using steady-state kinetics. The apparent kinetic data were obtained by varying the concentration of TMB or H₂O₂ while keeping the other one constant. A series of steady-state reaction rates were calculated and applied to the Lineweaver-Burk plot, $1/v = (K_m/V_{max}) \times (1/[S]) + 1/V_{max}$, where v is the initial velocity, K_m is the Michaelies-Menten constant, V_{max} is the maximal reaction velocity and $[S]$ is the concentration of the substrate.^{38-41, 44-49} The K_m and V_{max} were listed in Table S1. The results indicated the oxidation reaction catalyzed by MoS₂ nanosheets followed the typical Michaelies-Menten behavior.^{38, 40, 41, 44, 45, 49} towards both substrates, TMB and H₂O₂ (Fig.2). The double-reciprocal plots revealed the characteristic parallel lines of a ping-pong mechanism^{41, 44, 46-49} and implied that, like HRP, MoS₂ nanosheets bound and reacted with the first substrate and then released the first product before reacting with the second

substrate. To compare the catalytic activity of MoS₂ nanosheets with HRP, the steady-state kinetic assay of HRP were also

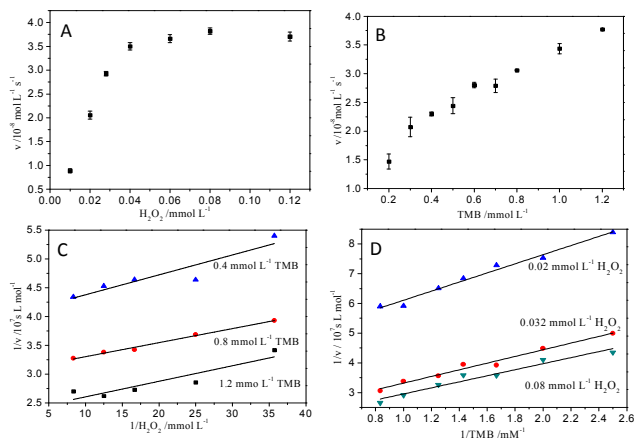


Fig.2 Steady-state kinetic assay and catalytic mechanism of MoS₂ nanosheets (A-D). The velocity (v) of the reaction was measured using MoS₂ nanosheets (1.8 $\mu\text{g mL}^{-1}$) in 0.5 mL Tris-HCl buffer (10 mmol L^{-1} , pH 6.9) at 30°C. The error bars represent the standard error derived from three repeated measurements. (A) The concentration of TMB was 1.2 mmol L^{-1} and H₂O₂ concentration was varied. (B) The concentration of H₂O₂ was 0.08 mmol L^{-1} and TMB concentration was varied. (C, D) Double reciprocal plots of activity of MoS₂ nanosheets with the concentration of one substrate (TMB or H₂O₂) fixed and the other varied.

performed (Fig.S7), the K_m and V_{max} for HRP were listed in Table S1. From Table S1, the apparent K_m value of MoS₂ nanosheets with H₂O₂ as the substrate was significantly lower than that of HRP, indicating that MoS₂ nanosheets has a higher activity to H₂O₂ than HRP. The apparent K_m value of MoS₂ nanosheets with TMB as the substrate was higher than that of HRP, consistent with the observation that a higher TMB concentration was needed to obtain the max activity of MoS₂ nanosheets.

Absorption spectra of TMB, MoS₂ nanosheets, and a fixed concentration of TMB (1.2 mmol L^{-1}) interacting with different concentrations of MoS₂ nanosheets were shown in Fig.S8. Pristine TMB exhibits almost no absorption at wavelength larger than 350 nm. As a result of interaction with the MoS₂ nanosheets, the absorption band at 385 nm shifts to 392 nm, accompanied by the hyperchromic effect at around 440 nm band. This result indicates charge-transfer interaction occurs between TMB and MoS₂ nanosheets, which is similar with the case between Few-Layer MoS₂ and Tetrathiafulvalene.⁵² Charge transfer from TMB to MoS₂ nanosheets is substantial and is partially associated with the p-type nature of few-layer MoS₂ material.⁵² It is thought that MoS₂ nanosheets could facilitate the electron transfer between TMB and H₂O₂ in the oxidation of TMB catalyzed by MoS₂ nanosheets. In this process, TMB molecules are absorbed on the surface of MoS₂ nanosheets and donate lone-pair electrons from the amino groups to MoS₂ nanosheets, which results in an increase in electron density and mobility in MoS₂ nanosheets. This would accelerate the electron transfer from MoS₂ nanosheets to H₂O₂, resulting in the reduction of H₂O₂ to H₂O in acid media and the increase of the reaction rate of TMB oxidation by H₂O₂.

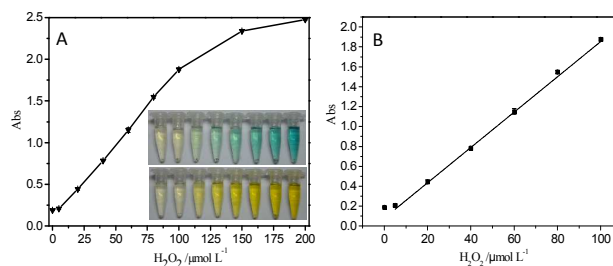
To further probe the catalytic mechanism of MoS₂ nanosheets, the catalytic reaction was further investigated at the presence of difference radical scavengers. As illustrated in Fig. S9, the absorbance was not effectively decreased at the presence of sodium azide (NaN₃) and superoxide dismutase (SOD), which were used as scavengers for ¹O₂⁵³ and O₂^{•-}⁵⁴

respectively. However, the absorbance was decreased greatly at the presence of ascorbic acid (AA) and thiourea, which were widely accepted as effective active oxygen free radical ($\cdot\text{OH}$ and O₂^{•-})⁵⁵ and $\cdot\text{OH}$ ⁵⁶ scavengers, respectively. These results revealed that $\cdot\text{OH}$ originated from the decomposition of H₂O₂ was produced in the reaction solution and contributed to the oxidation of TMB to form a blue product.

Based on the above, it is believed that MoS₂ nanosheets would facilitate the electron transfer between TMB and H₂O₂ and catalyze the decomposition of H₂O₂ in acid media into $\cdot\text{OH}$, which oxidizes TMB to form a blue product.

2.3 Detection of H₂O₂ and glucose

On these bases, a colorimetric method for the detection of H₂O₂ and glucose was developed by using the MoS₂ nanosheets-TMB-H₂O₂ system. Fig.3A showed a typical H₂O₂ concentration-response curve under optimal conditions. The linear range (Fig.3B) was from 5 to 100 $\mu\text{mol L}^{-1}$ ($R^2=0.9961$) with a detection limit of 1.5 $\mu\text{mol L}^{-1}$. Furthermore, the color variation for H₂O₂ response was also obvious by visual observation to as low as 5 $\mu\text{mol L}^{-1}$. In addition, other reactive oxygen species (ROS) were challenged for this catalytic



reaction. As shown in Fig. S10, this method might be applied to the detection of hydroxyl radical ($\cdot\text{OH}$), hypochlorite (ClO⁻). **Fig.3** (A) A dose-response curve for H₂O₂ detection and (B) the linear calibration plot for H₂O₂. Inset of Fig.3(A) were images of colored products for different concentrations of H₂O₂ before (top) and after (down) adding of 10 μL 20% (V/V) sulfuric acid. H₂O₂ concentration ($\mu\text{mol L}^{-1}$, from left to right): 0, 5, 20, 40, 60, 80, 100, 150.

Hydrogen peroxide is the main product of GOx-catalyzed reaction. When combined with glucose oxidase (GOx), the proposed colorimetric method could be used for the determination of glucose, which is an important indicator for the diagnosis of diabetes in clinical medicine.⁴⁷⁻⁴⁹ GOx catalyzed the oxidation of glucose to gluconic acid in Tris-HCl buffer solution and oxygen in solution was converted to H₂O₂, which would oxidize TMB to produce a blue-color product via the catalysis of MoS₂ nanosheets (Scheme 1). Fig.4A showed a typical glucose concentration-response curve. The linear range

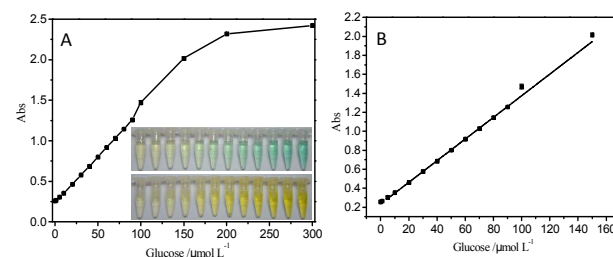


(Fig.4B) was from 5 to 150 $\mu\text{mol L}^{-1}$ ($R^2=0.9992$) with the limit of detection of 1.2 $\mu\text{mol L}^{-1}$.

Fig.4 (A) A dose-response curve for glucose detection and (B) the linear calibration plot for glucose. The error bars represent the standard deviation of three measurements. Inset of Fig.4(A) were images of colored products

for different concentrations of glucose before (top) and after (down) adding of 10 μL 20% (V/V) sulfuric acid. Glucose concentration ($\mu\text{mol L}^{-1}$, from left to right): 0, 1, 5, 10, 20, 30, 40, 50, 60, 70, 80, 90.

Furthermore, the color variation from yellow to blue was obvious on visual observation (Inset in Fig.4A), offering a convenient approach to detect glucose by the naked eyes even at low concentrations. The proposed method was applied to detect glucose in human serum samples (Fig.5), and the results agreed well with those obtained using the conventional enzymatic method (Table S2). Fructose, lactose, and maltose were used to investigate the selectivity of this method. The results (Fig.S11) demonstrated that the sensing system has a high selectivity for glucose detection.

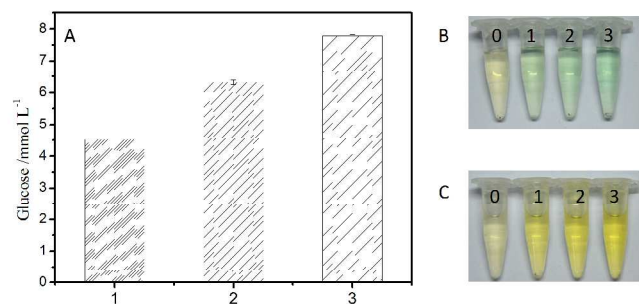
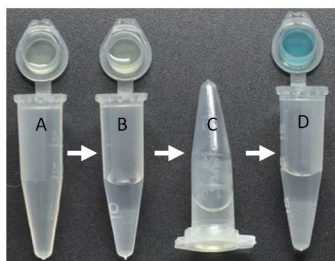


Fig.5 (A) The glucose concentration for diluted serum samples (1-3). Images of colored production for blank (0) and diluted serum samples (1-3) before (B) and after (C) adding of 10 μL 20% (V/V) sulfuric acid. Glucose concentration for serum samples: (1) 5.00 mmol L^{-1} , (2) 6.67 mmol L^{-1} , (3) 8.33 mmol L^{-1}

2.4 Visual detection of glucose using portable test kits

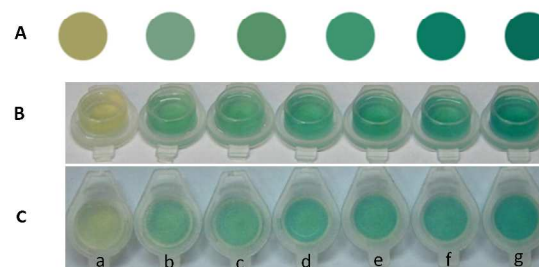
Although there are commercial instrument-based products for fast detection of serum glucose, the requirement of electric power and electronic read-out circuits makes the design complexity and the detection cost to increase. To facilitate the detection of serum glucose, a portable test kit for the visual detection of glucose was designed as a proof of concept by utilizing agarose hydrogel as a visual detection platform. Hydrogel is particularly suitable to design the visual detection platform due to its negligible background color and fluorescence emission, as well as large loading capacity and controllable shape.²⁷ All components of the test kit, including polypropylene microcentrifuge tubes, agarose, MoS₂ nanosheets, GOx, and water, are inexpensive, and the fabrication procedure is under ambient condition. The portable test kit was applied to evaluate glucose in the serum samples from normal persons and diabetes persons provided by the local



Scheme 2. Procedure for the detection of glucose in serum samples by a portable test kit. (A) opening the snap cap of test kit (pale yellow color in the hydrogel), (B) adding diluted serum sample solution to the test kit, (C) closing the snap cap and turning the test kit upside down before incubation at 37 $^{\circ}\text{C}$ for 60 min, (D) turning the test kit upside down again and opening

the snap cap to observe the color change of hydrogel (blue color in the hydrogel)

hospital. 30 μL of serum sample was diluted 30-fold with Tris-HCl buffer (10 mmol L^{-1} , pH 6.9). The detection procedure and the results were shown in Scheme 2 and Fig.6, respectively. The colors of hydrogel turned from pale yellow (blank) to yellow-green (< 8 mmol L^{-1} glucose in normal serum samples) or blue-green (> 8 mmol L^{-1} glucose in diabetes serum samples). The higher of the concentration of serum glucose, the deeper of the color of hydrogel. The general range of blood glucose concentration in healthy and diabetic persons is about 3-8 mmol L^{-1} and 9-40 mmol L^{-1} , respectively.^{48, 49} Thus, the portable test kit is applicable for instrument-free visual detection of glucose



in real serum samples.

Fig.6 (A) Standard colorimetric card for serum glucose (mmol L^{-1}) (from left to right: 0, 3, 5, 7, 9, 12) and photos of the hydrogel with different concentrations of serum glucose when opening the snap cap of the test kit (B) and closing the snap cap of the test kit (C). The concentration of glucose (mmol L^{-1}) in serum samples: (a) blank, (b) 5.00, (c) 5.31, (d) 6.98, (e) 7.2, (f) 8.49, (g) 11.88.

3. Conclusions

In summary, we have demonstrated that MoS₂ nanosheets possess an intrinsic peroxidase-like catalytic activity, which follows the typical Michaelies-Menten kinetics. MoS₂ nanosheets show a high catalytic activity over a wide pH (2.0-7.5). It is believed that MoS₂ nanosheets would facilitate the electron transfer between TMB and H₂O₂ and catalyse the decomposition of H₂O₂ in acid media into $\cdot\text{OH}$, which contributes to the oxidation of TMB to form a blue product. Using the catalytic activity of MoS₂ nanosheets and glucose oxidase (GOx), a highly selective and sensitive colorimetric assay for H₂O₂ and glucose was developed and a simple, cheap, portable test kit for serum glucose was constructed. Due to the observable color change from pale yellow to blue by the naked eyes, the visual detection of glucose in serum samples can be realized without any instrumentation or complicated designs. Only 30 μL of serum samples and simple dilution are needed, one can "see" the diabetes. It is anticipated that our study should facilitate applications of MoS₂ nanosheets in biotechnology and clinical diagnosis as peroxidase mimetic.

4. Experimental Section

4.1 Chemicals and Materials

MoS₂ nanosheets solution (18 mg/L, 1-8 monolayers, >99% purity in dry phase), which were prepared by solution-based exfoliation, were purchased from Nanjing XFNANO Materials Tech Co., Ltd (China). Tris(hydroxymethyl)methyl aminomethane (Tris), H₂O₂, thiourea, fructose and maltose were purchased from Sinopharm Chemical Reagent Co., Ltd. (China). Horseradish peroxidase (HRP, >150 U/mg), glucose oxidase (GOx), superoxide dismutase (SOD, 1750 U mg^{-1}),

glucose and lactose were obtained from Shanghai Sangon Biological Engineering Technology & Services Co., Ltd (China). 3,3',5,5'-tetramethylbenzidine (TMB), 2,2'-azino-bis(3-ethylbenzothiazoline-6-sulfonic acid) diammonium salt (ABTS) were bought from Bio Basic Inc (Canada). Agarose was bought from Shanghai Donghai Pharmaceutical Co., Ltd (China). *O*-phenylenediamine (OPD) and 0.5 mL clear polypropylene microcentrifuge tubes with snap caps were bought from Fuzhou DingGuo Biotechnology Co. Ltd (China). Sodium azide (NaN₃) and ascorbic acid (AA) were bought from Tianjin Fuchen and Xi'an chemical reagents factory (China), respectively.

4.2 Characterization of MoS₂ nanosheets

High-resolution transmission electron microscopy (HRTEM) images and TEM-based energy-dispersive X-ray (EDX) measurements were performed with an FEI Tecnai G2F20 transmission electron microscope. Field emission scanning electron microscopy (FE-SEM) and SEM-based EDX measurements were performed with an FEI Nova NanoSEM 230 field-emission scanning electron microscopy. All samples for FE-SEM and TEM measurements were deposited on a carbon film supported by copper grids. Atomic force microscopy (AFM) images were performed on a Multimode NanoScope IIIa scanning probe microscopy system (Bruker, USA). Samples for AFM imaging were prepared by depositing ethanol suspensions of MoS₂ nanosheets on a freshly cleaved mica surface. X-ray photoelectron spectroscopy (XPS) data were collected by a Thermo Scientific ESCALAB 250 with an Al K α source (1486.6 eV). Before XPS measurements the samples were deposited on a clean sheet of copper. Absorption spectra and kinetic measurements were carried out on a Lamda 750 UV-Vis-NIR spectrophotometer (PE, USA)

4.3 Detection of H₂O₂ and glucose

H₂O₂ detection was carried out as follows: 50 μ L MoS₂ nanosheets (18 μ g mL⁻¹), 50 μ L TMB (12 mmol L⁻¹) and 200 μ L Tris-HCl buffer (10 mmol L⁻¹, pH 6.9) were mixed. Then, 200 μ L H₂O₂ with different concentrations was added and the mixture was further incubated at 30 °C for 30 min. Finally, 10 μ L H₂SO₄ (20%, v v⁻¹) was added into the mixture to stop the reaction and the absorbance of the mixture was recorded at 450 nm.

Glucose detection was realized as follows: 20 μ L GOx (10 mg mL⁻¹) was added into 180 μ L Tris-HCl buffer (10 mmol L⁻¹, pH 6.9) containing different concentrations of glucose, and the mixture was incubated at 37 °C for 30 min to produce H₂O₂. The other detection procedure was the same as that of H₂O₂.

Before the detection of glucose in serum samples, the proteins in serum samples were removed by precipitation. 30 μ L of serum sample was diluted with 20 μ L water, and then 500 μ L Ba(OH)₂ (0.11 mol L⁻¹) and 500 μ L ZnSO₄ (0.0765 mol L⁻¹) were added. After centrifugation at 3880 rpm for 10 min, 200 μ L of supernatant solution was taken and diluted with Tris-HCl buffer (10 mmol L⁻¹, pH 6.9) to 1000 μ L. The other detection procedure was the same as that of glucose.

4.4 Preparation of portable test kits and visual detection of glucose in serum samples

A portable test kit for serum glucose was prepared as follows: agarose (20 mg) was completely dissolved in boiling water (2 mL) with stirring. When the solution was cooled down to 40 °C, 200 μ L MoS₂ nanosheets (18 μ g mL⁻¹), 300 μ L TMB (12 mmol L⁻¹), and 100 μ L GOx (10 mg mL⁻¹) were added.

After blended uniformly, the mixture solution (150 μ L) was transferred into the cap of microcentrifuge tube. The hydrogel was shaped after drying in ambient temperature for 5 min and the test kit was stored in the refrigerator at 4 °C before use. The test kits were stable at least for two weeks.

For the detection of glucose in serum samples, 30 μ L of serum sample was diluted with Tris-HCl buffer (10 mmol L⁻¹, pH 6.9) to 300 μ L and then added into the test kit. After closing the cap, the test kit was turned upside down to allow the infiltration of the sample solution into the hydrogel and incubated at 37 °C for 60 min. The color of the hydrogel turned from pale yellow to blue, which was dependence of the concentration of serum glucose.

Acknowledgements

The authors gratefully acknowledge NSFC (21177023) and Science Foundation of Fujian Province of China (2013J01044) for financial support.

Notes and references

Electronic Supplementary Information (ESI) available: See DOI: 10.1039/b000000x/

- J. N. Coleman, M. Lotya, A. O'Neill, S. D. Bergin, P. J. King, U. Khan, K. Young, A. Gaucher, S. De, R. J. Smith, I. V. Shvets, S. K. Arora, G. Stanton, H.-Y. Kim, K. Lee, G. T. Kim, G. S. Duesberg, T. Hallam, J. J. Boland, J. J. Wang, J. F. Donegan, J. C. Grunlan, G. Moriarty, A. Shmeliov, R. J. Nicholls, J. M. Perkins, E. M. Grievson, K. Theuwissen, D. W. McComb, P. D. Nellist and V. Nicolosi, *Science*, 2011, **331**, 568-571.
- H. S. S. R. Matte, A. Gomathi, A. K. Manna, D. J. Late, R. Datta, S. K. Pati and C. N. R. Rao, *Angew. Chem., Int. Ed.*, 2010, **49**, 4059-4062.
- Q. H. Wang, K. Kalantar-Zadeh, A. Kis, J. N. Coleman and M. S. Strano, *Nanotechnol.*, 2012, **7**, 699-712.
- K.-K. Liu, W. Zhang, Y.-H. Lee, Y.-C. Lin, M.-T. Chang, C.-Y. Su, C.-S. Chang, H. Li, Y. Shi, H. Zhang, C.-S. Lai and L.-J. Li, *Nano Lett.*, 2012, **12**, 1538-1544.
- Y. Yao, Z. Lin, Z. Li, X. Song, K.-S. Moon and C.-p. Wong, *J. Mater. Chem.*, 2012, **22**, 13494-13499.
- K. G. Zhou, N. N. Mao, H. X. Wang, Y. Peng and H. L. Zhang, *Angew. Chem. Int. Ed.*, 2011, **50**, 10839-10842.
- B. Radisavljevic, A. Radenovic, J. Brivio, V. Giacometti and A. Kis, *Nat. Nanotechnol.*, 2011, **6**, 147-150.
- J. Xiao, D. Choi, L. Cosimbescu, P. Koech, J. Liu and J. P. Lemmon, *Chem. Mater.*, 2010, **22**, 4522-4524.
- K. Chang and W. Chen, *ACS Nano*, 2011, **5**, 4720-4728.
- K. F. Mak, C. Lee, J. Hone, J. Shan and T. F. Heinz, *Phys. Rev. Lett.*, 2010, **105**, 136805.
- G. Eda, H. Yamaguchi, D. Voiry, T. Fujita, M. Chen and M. Chhowalla, *Nano Lett.*, 2011, **11**, 5111-5116.
- H. Wang, L. Yu, Y.-H. Lee, Y. Shi, A. Hsu, M. L. Chin, L.-J. Li, M. Dubey, J. Kong and T. Palacios, *Nano Lett.*, 2012, **12**, 4674-4680.
- V. K. Sangwan, H. N. Arnold, D. Jariwala, T. J. Marks, L. J. Lauhon and M. C. Hersam, *Nano Lett.*, 2013, **13**, 4351-4355.
- S. Kim, A. Konar, W.-S. Hwang, J. H. Lee, J. Lee, J. Yang, C. Jung, H. Kim, J.-B. Yoo and J.-Y. Choi, *Nat. Commun.*, 2012, **3**, 1011.
- H. Li, Z. Yin, Q. He, H. Li, X. Huang, G. Lu, D. W. H. Fam, A. I. Y. Tok, Q. Zhang and H. Zhang, *Small*, 2012, **8**, 63-67.
- R. V. Kashid, D. J. Late, S. S. Chou, Y.-K. Huang, M. De, D. S. Joag, M. A. More and V. P. Dravid, *Small*, 2013, **9**, 2730-2734.
- Z. Yin, H. Li, H. Li, L. Jiang, Y. Shi, Y. Sun, G. Lu, Q. Zhang, X. Chen and H. Zhang, *ACS Nano*, 2012, **6**, 74-80.
- D. J. Late, B. Liu, H. R. Matte, V. P. Dravid and C. Rao, *ACS Nano*, 2012, **6**, 5635-5641.
- K. Cho, W. Park, J. Park, H. Jeong, J. Jang, T.-Y. Kim, W.-K. Hong, S. Hong and T. Lee, *ACS Nano*, 2013, **7**, 7751-7758.
- D. J. Late, Y.-K. Huang, B. Liu, J. Acharya, S. N. Shirodkar, J. Luo, A. Yan, D. Charles, U. V. Waghmare, V. P. Dravid and C. N. R. Rao, *ACS Nano*, 2013, **7**, 4879-4891.

21. G. Berhault, D. I. R. M. Perez, A. Mehta, M. J. Yacaman and R. R. Chianelli, *Appl. Catal., A*, 2008, **345**, 80-88.
22. T. F. Jaramillo, K. P. Jørgensen, J. Bonde, J. H. Nielsen, S. Hørch and I. Chorkendorff, *Science*, 2007, **317**, 100-102.
23. Q. Xiang, J. Yu and M. Jaroniec, *J. Am. Chem. Soc.*, 2012, **134**, 6575-6578.
24. A. B. Laursen, S. Kegnaes, S. Dahl and I. Chorkendorff, *Energy Environ. Sci.*, 2012, **5**, 5577-5591.
25. T. Wang, H. Zhu, J. Zhuo, Z. Zhu, P. Papakonstantinou, G. Lubarsky, J. Lin and M. Li, *Anal. Chem.*, 2013, **85**, 10289-10295.
26. K. Saha, S. S. Agasti, C. Kim, X. Li and V. M. Rotello, *Chem. Rev.*, 2012, **112**, 2739-2779.
27. J. Du, L. Jiang, Q. Shao, X. Liu, R. S. Marks, J. Ma and X. Chen, *Small*, 2013, **9**, 1467-1481.
28. N. L. Rosi and C. A. Mirkin, *Chem. Rev.*, 2005, **105**, 1547-1562.
29. R. Elghanian, J. J. Storhoff, R. C. Mucic, R. L. Letsinger and C. A. Mirkin, *Science*, 1997, **277**, 1078-1081.
30. H. Otsuka, Y. Akiyama, Y. Nagasaki and K. Kataoka, *J. Am. Chem. Soc.*, 2001, **123**, 8226-8230.
31. R. Liu, R. Liew, J. Zhou and B. Xing, *Angew. Chem.*, 2007, **119**, 8955-8959.
32. K. Ai, Y. Liu and L. Lu, *J. Am. Chem. Soc.*, 2009, **131**, 9496-9497.
33. L. Guo, J. Zhong, J. Wu, F. Fu, G. Chen, X. Zheng and S. Lin, *Talanta*, 2010, **82**, 1654-1658.
34. J.-S. Lee, M. S. Han and C. A. Mirkin, *Angew. Chem.*, 2007, **119**, 4171-4174.
35. J. Du, Y. Sun, L. Jiang, X. Cao, D. Qi, S. Yin, J. Ma, F. Y. Boey and X. Chen, *Small*, 2011, **7**, 1407-1411.
36. J. Du, B. Zhu and X. Chen, *Small*, 2013, **9**, 4104-4111.
37. J. Du, Q. Shao, S. Yin, L. Jiang, J. Ma, X. Chen, *small*, **2012**, **8**, 3412-3416.
38. L. Ai, L. Li, C. Zhang, J. Fu and J. Jiang, *Chemistry*, 2013, **19**, 15105-15108.
39. X. Sun, S. Guo, C. S. Chung, W. Zhu and S. Sun, *Adv. Mater.*, 2013, **25**, 132-136.
40. J. Mu, Y. Wang, M. Zhao and L. Zhang, *Chem. Commun.*, 2012, **48**, 2540-2542.
41. L. Zhang, L. Han, P. Hu, L. Wang and S. Dong, *Chem. Commun.*, 2013, **49**, 10480-10482.
42. J. Xie, X. Zhang, H. Wang, H. Zheng and Y. Huang, *TrAC, Trends Anal. Chem.*, 2012, **39**, 114-129.
43. H. Wei and E. Wang, *Chem. Soc. Rev.*, 2013, **42**, 6060-6093.
44. L. Gao, J. Zhuang, L. Nie, J. Zhang, Y. Zhang, N. Gu, T. Wang, J. Feng, D. Yang and S. Perrett, *Nat. Nanotechnol.*, 2007, **2**, 577-583.
45. K. Cai, H. Han, Z. Lv, K. Chen, L. Huang, J. Wang, F. Shao and Y. Wang, *Chem. Commun.*, 2013, **49**, 6024-6026.
46. Y. Chen, H. Cao, W. Shi, H. Liu and Y. Huang, *Chem. Commun.*, 2013, **49**, 5013-5015.
47. L. Su, J. Feng, X. Zhou, C. Ren, H. Li and X. Chen, *Anal. Chem.*, 2012, **84**, 5753-5758.
48. Y. Song, K. Qu, C. Zhao, J. Ren and X. Qu, *Adv. Mater.*, 2010, **22**, 2206-2210.
49. W. Shi, Q. Wang, Y. Long, Z. Cheng, S. Chen, H. Zheng and Y. Huang, *Chem. Commun.*, 2011, **47**, 6695-6697.
50. S. Liu, J. Tian, L. Wang, Y. Luo and X. Sun, *RSC Adv.*, 2012, **2**, 411-413.
51. Y. Song, X. Wang, C. Zhao, K. Qu, J. Ren and X. Qu, *Chem. Eur. J.*, 2010, **16**, 3617-3621.
52. S. Dey, H. S. Matte, S. N. Shirodkar, U. V. Waghmare and C. N. Rao, *Chem. Asian J.*, 2013, **8**, 1780-1784.
53. J. R. Harbour and S. L. Issler, *J. Am. Chem. Soc.*, 1982, **104**, 903-905.
54. A. P. Schaap, A. L. Thayer, G. R. Faler, K. Goda and T. Kimura, *J. Am. Chem. Soc.*, 1974, **96**, 4025-4026.
55. Y. Tang, Y. Su, N. Yang, L. Zhang, and Yi Lv, *Anal. Chem.*, 2012, **84**, 5753-5758.
56. W. F. Wang, M. N. Schuchmann, H. P. Schuchmann, W. Knolle, J. V. Sonntag and C. V. Sonntag, *J. Am. Chem. Soc.*, 1999, **121**, 238-245.
57. Z. Yuan, N. Cai, Y. Du, Y. He and E. S. Yeung, *Anal. Chem.*, 2014, **86**, 419-426.